



Cite this: *Chem. Commun.*, 2016, 52, 7858

Received 26th February 2016,
Accepted 24th May 2016

DOI: 10.1039/c6cc01756h

www.rsc.org/chemcomm

Tunnelling in carbonic acid†

J. Philipp Wagner,^a Hans Peter Reisenauer,^a Viivi Hirvonen,^a Chia-Hua Wu,^b Joseph L. Tyberg,^b Wesley D. Allen^{*b} and Peter R. Schreiner^{*a}

The *cis,trans*-conformer of carbonic acid (H_2CO_3 , **1**, Fig. 1) generated by near-infrared radiation, undergoes an unreported quantum mechanical tunnelling rotamerization with half-lives in cryogenic matrices of 4–20 h, depending on temperature and host material. First-principles quantum chemistry at high levels of theory gives a tunnelling half-life of about 1 h, quite near those measured for the fastest rotamerizations.

Although carbonic acid (H_2CO_3 , **1**, Fig. 1) is constantly on the lips of millions in the form of carbonated beverages, evidence for the molecule in the gas phase was obtained only in 1987 by thermolysis of NH_4HCO_3 and mass spectrometric detection.¹ For many years this profoundly important molecule, which is considered essential for many biological processes,² escaped unequivocal identification in the gas phase. Indeed, it was vigorously debated whether H_2CO_3 could persist long enough to be spectroscopically identifiable, as the molecule decomposes readily into CO_2 and H_2O .³ At the same time, evidence was found for the existence of **1** in atmospheric clouds both on earth and several terrestrial planets.⁴ Finally, in 2009⁵ and 2011,⁶ Fourier-transform microwave spectroscopy provided the first spectroscopic characterization of gaseous H_2CO_3 , produced by passing a pulsed electric discharge of CO_2 in a supersonic jet through a water reservoir. The *cis-trans* (**1ct**)⁵ and *cis-cis* (**1cc**)⁶ rotamers (Fig. 1) were identified unequivocally, while the *trans-trans* (**1tt**) isomer was deemed unattainable because of its high relative energy and small rotational barrier ($1.8 \text{ kcal mol}^{-1}$ at CCSD(T)/CBS)⁷ to **1ct**.

Solid carbonic acid was first prepared in 1991 by high-energy irradiation of mixtures of carbon dioxide and water ice.^{8–10} Shortly thereafter, the protonation of potassium bicarbonate with excess HCl in glassy methanolic solutions led to a solid,

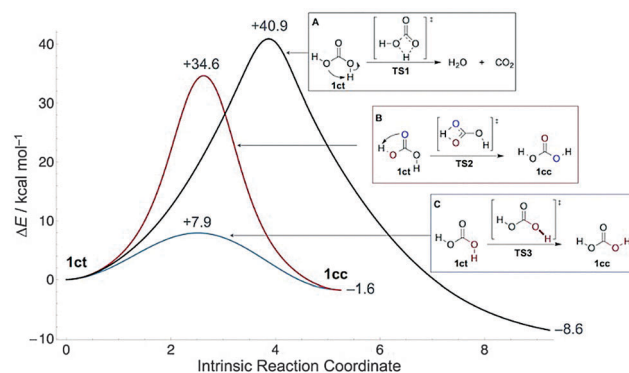


Fig. 1 Potential energy curves at CCSD(T)/CBS for disappearance of **1ct** by decomposition into H_2O and CO_2 (A), [1,3]hydrogen transfer (B), or internal C–O bond rotation (C). The profiles are drawn in terms of computed arc length (in $\text{u}^{1/2}$ bohr) along the intrinsic reaction path.

later termed the $\alpha\text{-H}_2\text{CO}_3$ polymorph.¹¹ An alternative $\beta\text{-H}_2\text{CO}_3$ polymorph was generated in an analogous fashion in aqueous glassy solutions in the presence of excess HBr, and conversion of $\beta\text{-H}_2\text{CO}_3$ to $\alpha\text{-H}_2\text{CO}_3$ was found upon treatment with HCl in methanol.¹² Overturning previous understandings, we proved recently⁷ through comparison of matrix-isolation^{13,14} infrared (IR) spectra of independently prepared compounds that the substance named $\alpha\text{-H}_2\text{CO}_3$ is in fact carbonic acid monomethyl ester,^{15,16} while only the β -polymorph^{17,18} is indeed solid H_2CO_3 .^{7,19} In doing so, we developed a novel synthetic route to gas-phase H_2CO_3 utilizing the ester pyrolysis of either Boc_2O or di-*t*-butyl carbonate, a conceptually simpler approach²⁰ generating much higher concentrations in the gas phase than previously achieved.

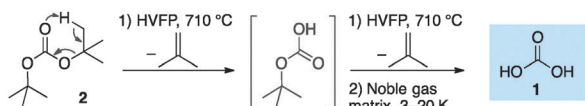
Carbonic acid is generally considered a fleeting molecule at ambient temperatures due to rapid decomposition into CO_2 and H_2O in the gas phase³ (Fig. 1) or deprotonation in solution. However, the gas-phase decomposition of **1** has a large barrier in excess of 40 kcal mol^{-1} ,^{21,22} because it is a thermally forbidden $[2_\sigma+2_\pi]$ cycloreversion. In the presence of water, an (auto)catalytic^{23–25} process appears to be operative instead: computations reveal that complexation of **1** with explicit water

^a Institute of Organic Chemistry, Justus-Liebig University, Heinrich-Buff-Ring 17, D-35392 Giessen, Germany. E-mail: prs@uni-giessen.de

^b Center for Computational Quantum Chemistry and Department of Chemistry, University of Georgia, Athens, Georgia 30602, USA. E-mail: wdallen@uga.edu

† Electronic supplementary information (ESI) available: Experimental procedures, detailed matrix isolation spectra, tables of assigned vibrational frequencies, the complete kinetic analysis, the theoretical methods, geometric structures, and electronic and zero-point energies. See DOI: 10.1039/c6cc01756h





Scheme 1 High-vacuum flash pyrolysis of di-*t*-butyl carbonate (**2**) and trapping of **1** in noble gas matrices.

molecules allows passage through more favourable cyclic transition states of six or more members that are lower in energy by 16–19 kcal mol^{−1}.²¹ Here we outline hitherto unreported conformational tunnelling of **1**, thereby capturing one of its key reactivities. The detailed delineation of the conformational, reactivity, and spectroscopic landscape of **1** will aid in its identification in the atmosphere and extraterrestrial environments.

Our highly efficient gas-phase preparation of **1** *via* ester pyrolysis (Scheme 1) and its trapping in noble gas matrices under cryogenic conditions allows the unimolecular kinetic behaviour to be probed.⁷ Di-*t*-butyl carbonate (**2**) readily undergoes double ester fragmentation *via* high vacuum flash pyrolysis (HVFP) with concomitant loss of two isobutene equivalents. Immediately after passing **2** through the pyrolysis tube, the products are trapped in noble gas matrices, kept at low temperatures (3–20 K), and monitored by means of IR spectroscopy. Bimolecular reactions do not occur because the trapped molecules are present in low concentrations and are fully surrounded by noble gas atoms (ratio *ca.* 1:10³); the solid noble gas matrices do not allow molecular diffusion.

Infrared bands for most vibrational modes of the two observable isomers of **1** were identified before.⁷ However, we were able to assign several new absorptions (Tables S16 and S17, ESI†), which assist the detection of **1** in extraterrestrial and other environments. The additional assignments include the $\nu_s(\text{O-C-O})$ symmetric stretching and $\delta(\text{O-C-O})$ deformation modes of both conformers, as well as the $\delta(\text{O-C=O})$ deformation of **1ct**. With decreasing polarizability of the noble gas host from Xe to Ne, we usually observe blue-shifted spectral features that slowly approach the gas-phase values for the vibrational transitions (Fig. S1, ESI†). On this basis it was also possible to assign the very close lying $\delta(\text{H-O-C}) + \nu_{\text{as}}(\text{O-C-O})$ vibrations of **1cc** and **1ct** (computed at 1183.8 and 1182.0 cm^{−1}, respectively) in neon in the theoretically predicted ordering.

After enrichment of the **1ct** conformer by narrow band NIR excitation (see ESI† for details) of matrices containing **1**, we observe its decay in solid Ne (3 K), Ar (3, 12.5, 17.5, 20 K), Kr (12.5 K), and Xe (12.5 K) with effective half-lives (τ_{eff}) of 4–20 h. During the kinetic measurements a long-pass IR filter cutting off all wavelengths below 4.5 μm (*ca.* 2200 cm^{−1}) was used to prevent unwanted photochemistry induced by the global radiation of the IR spectrometer. Decomposition of **1** into CO₂ and water (Fig. 1A) can be excluded, as we monitor the concomitant disappearance of **1ct** and appearance of **1cc**. Since the activation barriers for the other two possible processes (Fig. 1B and C) are too large to be overcome at cryogenic temperatures, quantum mechanical tunnelling (QMT)²⁶ must be responsible for the disappearance of **1ct**. The [1,3]H-shift of **1ct** to **1cc** (Fig. 1B) *via* TS2 exhibits a 34.6 kcal mol^{−1} barrier at the CCSD(T)/CBS level;

this compares well with the QCISD(T)/6-311++G(d,p)//MP2(full)/6-31++G(d,p) barrier of 34.3 kcal mol^{−1} reported earlier.²⁷ Barriers of this magnitude are not too large in principle to prohibit H-tunnelling on the time scales observed here, but in this case the potential energy profile is not “thin”,^{28–34} enough to make hydrogen transfer viable (Fig. 1). Unsurprisingly, we computed a prohibitive half-life of $\tau = 4.4 \times 10^6$ y for this reaction along a CCSD(T)/cc-pVQZ//MP2/aug-cc-pVTZ minimum energy path within a Wenzel–Kramers–Brillouin (WKB) tunnelling model^{35,36} that has proved very accurate for H-transfer reactions.^{28,37}

The isomerization of **1ct** through C–O single bond rotation has a barrier of only 7.9 kcal mol^{−1} (Fig. 1), which is in the 2–13 kcal mol^{−1} range typical of carboxylic acids^{38–44} but still much too large to be overcome thermally at the temperatures of our experiments. Hence, the decay of **1ct** to **1cc** must occur *via* tunnelling rotational isomerization, a generic fundamental property of carboxylic acids.^{38–44} We executed a detailed kinetic analysis of this tunnelling phenomenon in different noble gases and at various temperatures (Table 1).

The intricate kinetic behaviour of matrix-isolated **1** was treated within a multi-exponential model we recently developed to describe a similar conformational tunnelling process in oxalic acid, termed domino tunnelling.⁴⁵ To achieve high-quality fits of the data within the experimental error bars, the assumption of three classes of matrix-isolated carbonic acid molecules was required: a frozen class, in which tunnelling is entirely precluded by the environment; a slow class with seemingly hindered conformational tunnelling and half-lives (τ_1) of 11–26 h; and a fast class, characterized by half-lives (τ_2) of 2–5 h, for which the matrix atoms appear to interfere to only a limited extent with the conformational tunnelling. We emphasize here that our three-class model is phenomenological in nature, although it is appealing to interpret the experimental results in terms of a hindering matrix environment that softens at higher temperatures. The final kinetic analysis employed two half-lives (τ_1 , τ_2) and three initial population ratios (**1ct** fast: slow, **1ct** frozen: slow, and total **1ct**: **1cc**) as fitting parameters in a simultaneous, nonlinear least-squares fit of all suitable infrared spectral bands of both **1ct** and **1cc**. Complete details of the kinetic analysis are given in the ESI† along with plots of the data and fits. Deuteration completely suppresses the tunnelling

Table 1 Tunnelling half-lives τ (in h) in solid noble gas matrices at several temperatures. X_{frozen} , X_{fast} , and X_{slow} are the mole fractions for the frozen ($\tau = \infty$), slow (τ_1), and fast (τ_2) classes of trapped molecules of **1ct**, respectively^a

Matrix (T/K)	τ_1	τ_2	τ_{eff}^b	X_{frozen}	X_{slow}	X_{fast}
Ar (3)	19.7(1)	—	19.7	0.61	0.39	0
Ar (12.5)	13(2)	4(9)	12.5	0.29(7)	0.69(7)	0.03(9)
Ar (17.5)	12(2)	4.8(7)	7.6	0	0.46(17)	0.54(17)
Ar (20)	14(3)	3.0(2)	4.4	0	0.31(6)	0.69(6)
Ne (3)	25.7(4)	2.0(4)	19.8	0.31	0.61	0.08
Kr (12.5)	16(6)	5(4)	10.5	0.26(23)	0.57(18)	0.17(25)
Xe (12.5)	11.2(8)	2.4(5)	5.9	0.53(2)	0.36(1)	0.11(3)

^a Standard errors of fits to experimental data in parentheses in units of the last significant digit. ^b Time required for fitted relative population function to fall half of its descent.



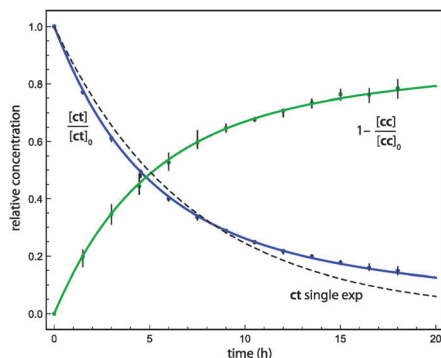


Fig. 2 Time evolution of H_2CO_3 conformer concentrations in an Ar matrix at 20 K after NIR irradiation. Blue and green curves result from the global, nonlinear least-squares fit of the multi-exponential kinetic model to three and five IR bands of **1ct** and **1cc**, respectively. The dashed curve is the best single-exponential fit for **1ct**.

isomerization, and we compute $\tau = 2400$ y for monodeuterated **1** (see ESI†); no tunnelling of deuterated **1** was observed over one day at 20 K in Ar.

The Ar (20 K) results shown in Fig. 2 are representative of our kinetic analysis of conformational tunnelling. A single-exponential fit to the **1ct** decay profile yields an effective half-life of 4.4 h, but the poor quality of the fit demonstrates the multi-exponential character of the kinetics. The initial ratio of fast:slow sites is near two, and in this case the data do not support the presence of frozen sites ($X_{\text{frozen}} = 0$). The slow and fast tunnelling of **1ct** exhibits the half-lives $\tau_1 = 14 \pm 3$ h and $\tau_2 = 3.0 \pm 0.2$ h, respectively.

To theoretically support our experiments, a distinguished reaction path (DRP) was generated for **1ct** \rightarrow **1cc** by a series of MP2/aug-cc-pVTZ constrained geometry optimizations, whereby the torsion angle $\tau_{\text{O}=\text{C}-\text{O}-\text{H}}$ was varied in 5° increments between 0° and 180° while all other internal coordinates were optimized. Along this path, CCSD(T)/CBS energies were computed to obtain an accurate potential energy curve for the isomerization. Finally, a DRP projected frequency analysis⁴⁶ was employed to evaluate harmonic vibrational frequencies (ω_i) and zero-point vibrational (ZPVE) corrections for each value of $\tau_{\text{O}=\text{C}-\text{O}-\text{H}}$. Tunnelling probabilities (κ) for **1ct** \rightarrow **1cc** were computed using exact numerical integration⁴⁵ and the WKB approximation.³⁵ Tunnelling rates were evaluated as the product of the transmission probability κ and the classical rate (ω_0) at which the reactant hits the barrier, assuming that the collision energy under cryogenic conditions is the reaction-mode ZPVE of $\omega_0/2$. The computed intrinsic tunnelling half-lives (τ_0) for the **1ct** \rightarrow **1cc** isomerization in the gas-phase amount to 56 min employing exact numerical integration and to 72 min within the WKB approximation. In support of the methodology underlying these results, a systematic computational study on acid tunnelling has found that “the minimum energy path can be considered as a good approximation for the *cis*-to-*trans* tunneling path with maximum transparency”.⁴⁷ Although our initial tunnelling computations do not incorporate reaction-path curvature effects that would further enhance the rate,^{48,49} the results compare well with the fast components (τ_2) obtained from the multi-exponential kinetic analysis of our experiments. Importantly, the X_{fast} mole fractions increase toward

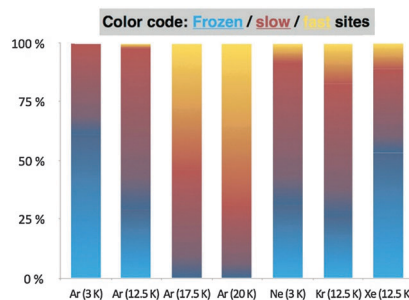


Fig. 3 Mole fractions of frozen, slow, and fast tunnelling sites in different noble gas matrices at several temperatures.

1 and the τ_{eff} values diminish toward τ_0 upon elevating the temperature of the Ar matrix (Table 1 and Fig. 3). While a rigorous assessment of various theoretical methods for computing tunnelling rates is beyond the scope of this communication, we report additional predictions of half-lives obtained with the ZCT and SCT approaches implemented in POLYRATE in the ESI.†^{50–52}

The complicated observed tunnelling behaviour is presumably attributable to varying degrees in which the matrix environment hinders the rotamerization of **1**. The thermal energy of our highest-temperature experiments (20 K) is not sufficient to significantly excite the C–O torsional vibration (491 cm^{-1} , CCSD(T)/cc-pVTZ) to accelerate the tunnelling rotamerization, which would only become important at about 60 K; however, there is enough thermal energy to excite the solid noble gas host material, whose Debye frequencies are in the range of $40\text{--}70\text{ cm}^{-1}$.⁵³ As the matrix softens at higher temperatures, it can better accommodate the structural changes required for tunnelling of **1ct**. Such temperature dependences of conformational tunnelling processes have already been observed experimentally⁵⁴ and rationalized through a theoretical study of the noble gas environment,⁵⁵ which showed that the temperature dependence of the tunnelling event is most likely attributable to a reorganization of the matrix environment. The circumstances are very different for the highly exothermic tunnelling of hydroxycarbenes to the corresponding aldehydes.^{32,37}

The intricate dependence of QMT on the noble gas host is currently not fully understood (Fig. 3). Argon seems in this respect well behaved as tunnelling accelerates with increasing temperature in the 3–20 K temperature regime; this corresponds well with a temperature-dependent activation of the noble gas atoms during the QMT rotamerization. Krypton is comparable, while the most polarizable Xe-matrix impedes tunnelling. Comparison with the Ne-matrix is difficult, but its low polarizability is likely to reduce the interaction with the interconverting conformers relative to Ar at the same temperature. Such behaviour has been reported before, *e.g.*, in the conformational tunnelling of formic acid that exhibits increasing tunnelling rates in going from Xe to Ne, while its *O*-deuterated isotopologue shows the opposite trend.⁵⁶

In terms of competing tunnelling mechanisms, it is clear that while the two possible pathways from **1ct** to **1cc** *via* **TS2** and **TS3**, respectively, have approximately the same width (Fig. 1), the tunnelling probabilities are primarily determined by barrier height, as found in classic kinetically controlled reactions.



This situation is in marked contrast to the phenomenon of tunnelling control,³² where barrier width trumps barrier height in favour of the thermodynamic product. The 26.7 kcal mol⁻¹ activation barrier difference between the two transition structures translates into a tunnelling rate ratio of approximately 1:10¹⁰, *i.e.*, essential quantitative selectivity.

We have unveiled a novel conformational tunnelling isomerization of **1** (in the range of 4–20 h) that is supported by high-level quantum chemical computations. The tunnelling process strongly depends on the temperature and nature of the matrix environment. The three phenomenological classes of tunnelling sites demonstrate that tunnelling is affected by the environment and therefore can in principle be controlled externally. On the basis of these findings and the theoretical predictions, we expect the tunnelling half-life for the isomerization of **1ct** to **1cc** would be even faster in the gas phase.

This work was supported by a collaboration grant from the U.S. National Science Foundation (CHE-1124885) and the Deutsche Forschungsgemeinschaft (Schr 597/18-1) to W. D. A. and P. R. S.; V. H. thanks the Liebig College at Justus-Liebig University, sponsored by the State of Hesse.

Notes and references

- 1 J. K. Terlouw, C. B. Lebrilla and H. Schwarz, *Angew. Chem., Int. Ed. Engl.*, 1987, **26**, 354–555.
- 2 K. Adamczyk, M. Prémont-Schwarz, D. Pines, E. Pines and E. T. J. Nibbering, *Science*, 2009, **326**, 1690–1694.
- 3 S. Ghoshal and M. K. Hazra, *RSC Adv.*, 2015, **5**, 17623–17635.
- 4 C. J. Bennett, C. P. Ennis and R. I. Kaiser, *Astrophys. J.*, 2014, **794**, 57.
- 5 T. Mori, K. Suma, Y. Sumiyoshi and Y. Endo, *J. Chem. Phys.*, 2009, **130**, 204308.
- 6 T. Mori, K. Suma, Y. Sumiyoshi and Y. Endo, *J. Chem. Phys.*, 2011, **134**, 044319.
- 7 H. P. Reisenauer, J. P. Wagner and P. R. Schreiner, *Angew. Chem., Int. Ed.*, 2014, **53**, 11766–11771.
- 8 M. H. Moore and R. K. Khanna, *Spectrochim. Acta, Part A*, 1991, **47**, 255–262.
- 9 W. Zheng and R. I. Kaiser, *Chem. Phys. Lett.*, 2007, **450**, 55–60.
- 10 M. Garozzo, D. Fulvio, O. Gomis, M. E. Palumbo and G. Strazzulla, *Planet. Space Sci.*, 2008, **56**, 1300–1308.
- 11 W. Hage, A. Hallbrucker and E. Mayer, *J. Am. Chem. Soc.*, 1993, **115**, 8427–8431.
- 12 W. Hage, A. Hallbrucker and E. Mayer, *J. Chem. Soc., Faraday Trans.*, 1995, **91**, 2823–2826.
- 13 T. Bally, in *Reactive Intermediates*, ed. R. A. Moss, M. S. Platz and M. Jones Jr., Wiley-Interscience, Hoboken, New Jersey, 2004, pp. 797–845.
- 14 A. Barnes, W. J. Orville-Thomas, R. Gaufrès and A. Müller, *Matrix Isolation Spectroscopy*, D. Reidel Publishing Company, Dordrecht, 1981.
- 15 A. Dibeneditto, M. Aresta, P. Giannoccaro, C. Pastore, I. Pápai and G. Schubert, *Eur. J. Inorg. Chem.*, 2006, 908–913.
- 16 J. Bernard, *Faculty of Chemistry and Pharmacy*, PhD thesis, University of Innsbruck, Innsbruck, 2014, p. 160.
- 17 I. Kohl, K. Winkel, M. Bauer, K. R. Liedl, T. Loerting and E. Mayer, *Angew. Chem., Int. Ed.*, 2009, **48**, 2690–2694.
- 18 S. K. Reddy and S. Balasubramanian, *Chem. Commun.*, 2014, **50**, 503–514.
- 19 G. Bucher and W. Sander, *Science*, 2014, **346**, 544–545.
- 20 G. Bucher, *Eur. J. Org. Chem.*, 2010, 1070–1075.
- 21 T. Loerting, C. Tautermann, R. T. Kroemer, I. Kohl, A. Hallbrucker, E. Mayer and K. R. Liedl, *Angew. Chem., Int. Ed.*, 2000, **39**, 891–894.
- 22 B. Jonsson, G. Karlstrom, H. Wennerstrom, S. Forsen, B. Roos and J. Almlof, *J. Am. Chem. Soc.*, 1977, **99**, 4628–4632.
- 23 S. Ghoshal and M. K. Hazra, *J. Phys. Chem. A*, 2014, **118**, 2385–2392.
- 24 M. Kumar, D. H. Busch, B. Subramaniam and W. H. Thompson, *J. Phys. Chem. A*, 2014, **118**, 5020–5028.
- 25 M. Kumar, D. H. Busch, B. Subramaniam and W. H. Thompson, *J. Phys. Chem. A*, 2014, **118**, 10155–10156.
- 26 J. Kästner, *Wiley Interdiscip. Rev.: Comput. Mol. Sci.*, 2014, **4**, 158–168.
- 27 C. A. Wight and A. I. Boldyrev, *J. Phys. Chem.*, 1995, **99**, 12125–12130.
- 28 J. Kästner, *Chem. – Eur. J.*, 2013, **19**, 8207–8212.
- 29 B. K. Carpenter, *J. Am. Chem. Soc.*, 1983, **105**, 1700–1701.
- 30 B. K. Carpenter, *Science*, 2011, **332**, 1269–1270.
- 31 M. Ertelt, D. A. Hrovat, W. T. Borden and W. Sander, *Chem. – Eur. J.*, 2014, **20**, 4713–4720.
- 32 P. R. Schreiner, H. P. Reisenauer, D. Ley, D. Gerbig, C.-H. Wu and W. D. Allen, *Science*, 2011, **332**, 1300–1303.
- 33 S. Kozuch, *Org. Lett.*, 2014, **16**, 4102–4105.
- 34 S. Kozuch, *Phys. Chem. Chem. Phys.*, 2014, **16**, 7718–7727.
- 35 H. A. Kramers, *Z. Phys.*, 1926, **39**, 828–840.
- 36 M. Razavy, *Quantum Theory of Tunneling*, World Scientific, Singapore, 2003.
- 37 P. R. Schreiner, H. P. Reisenauer, F. C. Pickard Iv, A. C. Simmonett, W. D. Allen, E. Matyus and A. G. Császár, *Nature*, 2008, **453**, 906–909.
- 38 M. Pettersson, E. M. S. Macoas, L. Khriachtchev, J. Lundell, R. Fausto and M. Räsänen, *J. Chem. Phys.*, 2002, **117**, 9095–9098.
- 39 E. M. S. Macoas, L. Khriachtchev, R. Fausto and M. Räsänen, *J. Phys. Chem. A*, 2004, **108**, 3380–3389.
- 40 S. Amiri, H. P. Reisenauer and P. R. Schreiner, *J. Am. Chem. Soc.*, 2010, **132**, 15902–15904.
- 41 G. Bazsó, S. Gobi and G. Tarczay, *J. Phys. Chem. A*, 2012, **116**, 4823–4832.
- 42 G. Bazsó, G. Magyarfalvi and G. Tarczay, *J. Phys. Chem. A*, 2012, **116**, 10539–10547.
- 43 G. Bazsó, E. E. Najbauer, G. Magyarfalvi and G. Tarczay, *J. Phys. Chem. A*, 2013, **117**, 1952–1962.
- 44 D. Gerbig and P. R. Schreiner, *J. Phys. Chem. B*, 2014, **119**, 693–703.
- 45 P. R. Schreiner, J. P. Wagner, H. P. Reisenauer, D. Gerbig, D. Ley, J. Sarka, A. G. Császár, A. Vaughn and W. D. Allen, *J. Am. Chem. Soc.*, 2015, **137**, 7828–7834.
- 46 W. D. Allen, A. Bodi, V. Szalay and A. G. Császár, *J. Chem. Phys.*, 2006, **124**, 224310.
- 47 M. Tsuge and L. Khriachtchev, *J. Phys. Chem. A*, 2015, **119**, 2628–2635.
- 48 Y. P. Liu, G. C. Lynch, T. N. Truong, D. H. Lu, D. G. Truhlar and B. C. Garrett, *J. Am. Chem. Soc.*, 1993, **115**, 2408–2415.
- 49 T. V. Albu, B. J. Lynch, D. G. Truhlar, A. C. Goren, D. A. Hrovat, W. T. Borden and R. A. Moss, *J. Phys. Chem. A*, 2002, **106**, 5323–5338.
- 50 A. Kuppermann and D. G. Truhlar, *J. Am. Chem. Soc.*, 1971, **93**, 1840–1851.
- 51 R. T. Skodje, D. G. Truhlar and B. C. Garrett, *J. Phys. Chem.*, 1981, **85**, 3019–3023.
- 52 J. Zheng, S. Zhang, B. J. Lynch, J. C. Corchado, Y.-Y. Chuang, P. L. Fast, W.-P. Hu, Y.-P. Liu, G. C. Lynch, K. A. Nguyen, C. F. Jackels, A. F. Ramos, B. A. Ellingson, V. S. Melissas, J. Villà, I. Rossi, E. L. Coitiño, J. Pu, T. V. Albu, A. Ratkiewicz, R. Steckler, B. C. Garrett, A. D. Isaacson and D. G. Truhlar, *POLYRATE 2010-A: Computer Program for the Calculation of Chemical Reaction Rates for Polyatomics.*, 2010.
- 53 H. J. Jodl, in *Chemistry and Physics of Matrix-Isolated Species*, ed. L. Andrews and M. Moskovits, 1989.
- 54 E. M. S. Macoas, L. Khriachtchev, M. Pettersson, R. Fausto and M. Räsänen, *J. Chem. Phys.*, 2004, **121**, 1331–1338.
- 55 L. I. Trakhtenberg, A. A. Fokeyev, A. S. Zyubin, A. M. Mebel and S. H. Lin, *J. Chem. Phys.*, 2009, **130**, 144502.
- 56 A. Domanskaya, K. Marushkevich, L. Khriachtchev and M. Räsänen, *J. Chem. Phys.*, 2009, **130**, 154509.

